JOURNAL OF GEOPHYSICAL RESEARCH, VOL. 93, NO. B6, PAGES 6419-6429, JUNE 10, 1988

Thermal Contraction and the State of Stress in the Oceanic Lithosphere

WILLIAM F. HAXBY

Lamont-Doherty Geological Observatory, Palisades, New York

E. M. PARMENTIER

Department of Geological Sciences, Brown University, Providence, Rhode Island

Nonuniform contraction of the oceanic lithosphere as it cools and thickens following its formation at the axis of a spreading center results in a complex three-dimensional state of deviatoric stress which can be separated into two parts: a thermal bending stress due to changes in the vertical temperature distribution and a thermal contraction stress due to lateral variations in the vertically averaged temperature. We examine thermal contraction stresses due to temperature changes in a thin, semi-infinite rectangular plate bounded by the spreading center axis. Two stress-free boundaries, representing transforms or fracture zones, define the plate width or ridge segment length L. With the bottom of the elastic plate defined by a prescribed temperature, the plate thickens as the square root of age, as expected for a thermal boundary layer due to vertical conductive cooling. Above this prescribed temperature, elastic stresses are assumed to relax quickly. Stresses are obtained by properly accounting for the rate of accumulation of the vertically averaged stress as initially stress-free material is added to bottom of the cooling, thickening plate. The state of thermal contraction stress calculated from this model is characterized by large tensile stresses at the boundaries of the plate and relatively low stresses in the plate interior. At the ridge axis, ridge-parallel tensile stresses are about 300 MPa, the same as if the plate were not allowed to contract in this direction. Along the transform boundary, the maximum transform-parallel tensile stress occurs at a distance $L/2$ from the ridge-transform intersection, where its magnitude is comparable to the stress at the ridge axis. The tangential stresses at the plate boundary decrease rapidly with distance from the boundary; at a distance of $L/4$ from the ridge axis the ridge axis parallel stresses are one tenth of their ridge axis magnitude. The stress magnitudes are independent of both spreading rate and ridge segment length. A large transform-parallel tensile stress may control the length of transform offsets. Thermal bending moments are influenced by the large thermal contraction stresses near the ridge axis. However, a short distance from the ridge these moments attain their free horizontal contraction values which previous studies have shown to cause observable bending of the plate and a geoid anomaly at fracture zones. Flexure due to thermal bending moments will concentrate bending stresses at a distance from the fracture zone determined by the flexural length of the plate, thus providing a natural length scale controlling the spacing of transforms.

INTRODUCTION

Contraction of cooling oceanic lithosphere has important implications for our understanding of the seafloor spreading process and the tectonic evolution of oceanic lithosphere. While vertical thermal contraction is expressed in the subsidence of seafloor with age, horizontal thermal contraction can produce large stresses. Thermal stresses that are as large as theoretical models predict will contribute significantly to the state of intraplate stress in the oceanic lithosphere. The existence of large thermal stresses is indicated both by studies of intraplate seismicity [*Bergman and Solomon*, 1984; *Wiens and Stein*, 1984; *Bratt et al.*, 1985] and by geoid anomalies at fracture zones [*Parmentier and Haxby*, 1986]. These stresses may have a variety of important consequences. For example, thermal stresses may strongly influence the degree to which intraplate stresses reflect plate driving forces [*Sykes and Sbar*, 1974; *Richardson et al.*, 1979; *Wiens and Stein*, 1983]. The contribution of thermal stress to geoid anomalies at fracture zones may affect measurements of the change in geoid height across fracture zones and the geoid height-age relationship and mantle thermal structure that have been inferred in this way [*Crough*, 1979; *Detrick*, 1981; *Sandwell and Schubert*, 1982; *Cazanave et al.*, 1983]. A good understanding of the form of the geoid anomaly is also needed for properly identifying fracture zones and for plate motion reconstructions based on fracture zone traces identified from geoid anomalies [*Haxby et al.*, 1985]. *Lister* [1986] has suggested that thermal stresses may be an important factor in magmatic and hydrothermal processes. More generally, thermal stresses may play an important role in intraplate tectonics. For example, *Turcotte and Oxburgh* [1973] have suggested that thermal stress may explain the formation of island and seamount chains. At plate boundaries, thermal stresses may in some way be responsible for the formation of transform faults and fracture zones (FZs) along mid-ocean ridges [*Collette*, 1974; *Turcotte*, 1974; *Sandwell*, 1986].

Thermal stresses can be conveniently separated into two parts, the first due to changes in the temperature variation with depth and the second due to changes in the vertically averaged temperature. We will refer to these two contributions as thermal bending stresses and thermal contraction stresses, respectively. In a recent study [*Parmentier and Haxby*, 1986] we examined thermal bending stresses in thickening, cooling oceanic lithosphere. Flexure of the oceanic lithosphere at fracture zones should occur in response to these bending stresses, and the resulting seafloor topography should produce visible geoid anomalies. We showed that bending of the lithosphere by thermal stresses can explain important characteristics of

Paper number 7B6053.
0148-0227/88/007B-6053$05.00

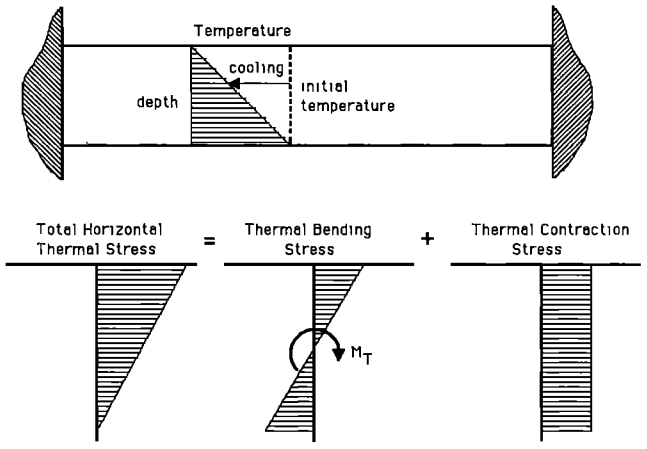

Fig. 1. Simple example showing thermal stresses in an elastic plate due to nonuniform cooling. The stresses can be separated into two additive parts. The thermal contraction stresses represent the thickness-averaged stress in the plate. The thermal bending stresses, representing the stress variation over the thickness of the plate, introduce a moment M_T that will tend to bend the plate. If the plate were not horizontally constrained and so free to contract, the thermal contraction stress would vanish, but the thermal bending stresses, representing only the differential contraction between the top and bottom of the plate, would remain unchanged.

the observed geoid anomaly at FZs. A geoid high that occurs persistently on the old side of FZs, discussed later, can be explained by flexure due to thermal bending stresses. This geoid anomaly may provide direct evidence for the magnitude and depth distribution of thermal stresses in the oceanic lithosphere.

The simple example shown in Figure 1 illustrates the distinction between thermal contraction and thermal bending stresses. Consider an initially unstressed elastic plate that is constrained at its ends so that it cannot contract horizontally. If the plate is cooled nonuniformly over its thickness, a horizontal thermal stress will develop that is proportional to the amount of cooling at a given depth. In general, the total horizontal thermal stress can be separated into two parts, the thermal contraction stresses and the thermal bending stresses. The thermal contraction stresses are simply the depth-averaged stresses in the plate and, by definition, are uniform with depth. The variation of stress with depth is reflected in the thermal bending stresses which exert a moment M_T about the center plane of the plate. If the plate were not constrained and thus free to contract horizontally, the thermal contraction stresses would vanish. The remaining thermal bending stresses due to differential cooling with depth would bend the plate. In a perfectly elastic material the total state of stress can be simply represented as the additive superposition of the thermal contraction and thermal bending stresses. In this case the thermal contraction stresses would not affect the thermal bending moment.

Thermal stresses in the oceanic lithosphere must differ from this simple example in two important respects. First, assuming that elastic stress relaxes rapidly above a prescribed temperature that defines the bottom of a brittle-elastic plate, thermal stress accumulates progressively as the plate cools and thickens by the addition of unstressed material at its base. Second, the accumulating thermal stresses beecome large enough that the plate fails by faulting. Thermal stress distributions for the limiting cases of free horizontal contraction and no horizontal contraction are shown in Figure 2, taken from *Parmentier and Haxby* [1986]. The maximum stresses are limited by brittle failure of the plate along the dashed failure envelopes shown. The distinctly different distribution of stresses in the two cases results in a large difference in the thermal bending moments [see *Parmentier and Haxby*, 1986, Figure 2]. In the free contraction case the vertically averaged thermal stress, or thermal contraction stress, vanishes. In the no-horizontal contraction case, as considered by *Turcotte* [1974], the thermal contraction stress does not vanish, and the corresponding thermal bending moment is much smaller than in the free contraction case. For a plate in which thermal stresses accumulate progressively as the plate thickens and which undergoes brittle failure, the magnitude of the thermal bending moment is strongly affected by the thermal contraction stresses.

In this study we examine thermal contraction stresses in the oceanic lithosphere by considering the problem of an elastic plate that thickens with age or distance from an accreting plate boundary. In addition to assessing the effect of thermal contraction stresses on the thermal bending moment, it is important to consider these stresses to understand the complete state of thermal stress in the oceanic lithosphere and its possible implications for intraplate seismicity, structures observed on the seafloor, and the mechanism(s) responsible for the formation of FZs.

THEORETICAL FORMULATION

We consider the simple problem of a plate of finite width L that thickens with distance from a spreading center ($x = 0$), as shown in Figure 3. In the x direction, perpendicular to the spreading center, the plate is taken to be infinitely long. Normal and shear stresses are assumed to vanish along the edges of the plate at $y = \pm L/2$ and at $x = 0$. We assume that rock behaves as an elastic material for temperatures below a prescribed temperature T_l, but that above this temperature, elastic stresses relax instantaneously. The plate thickens as the square root of age or distance from the spreading center, as would be predicted by vertical conductive cooling and which is consistent with the observed seafloor depth-age relationship for young oceanic lithosphere. In this case the temperature distribution is given by $T(x,z) = T_m \text{ erf } (z/2(\kappa x/U)^{1/2})$, and the thickness of the plate becomes $h = 2A(\kappa x/U)^{1/2}$, where $\text{erf } (A) = T_l/T_m$, κ is the thermal diffusivity, and U is the half-spreading rate.

In a material with coefficient of linear thermal expansion α, a uniform temperature change δT would produce a strain $\alpha\delta T$ in each of any three orthogonal directions and a volume change of $3\alpha\delta T$. However, in a body of material that cools nonuniformly, differences in thermal volume change between adjacent material elements will cause thermal stresses. These stresses must satisfy the equilibrium equations, and the resulting strains must satisfy the strain compatibility conditions [cf. *Timoshenko and Goodier*, 1970]. With suitably prescribed stress or displacement boundary conditions the thermal stress field within an elastic body can be calculated by solving simultaneously the constituitive equations, the equilibrium equations, and the compatibility conditions. In the present problem this would lead to a complicated three-dimensional stress field within the plate.

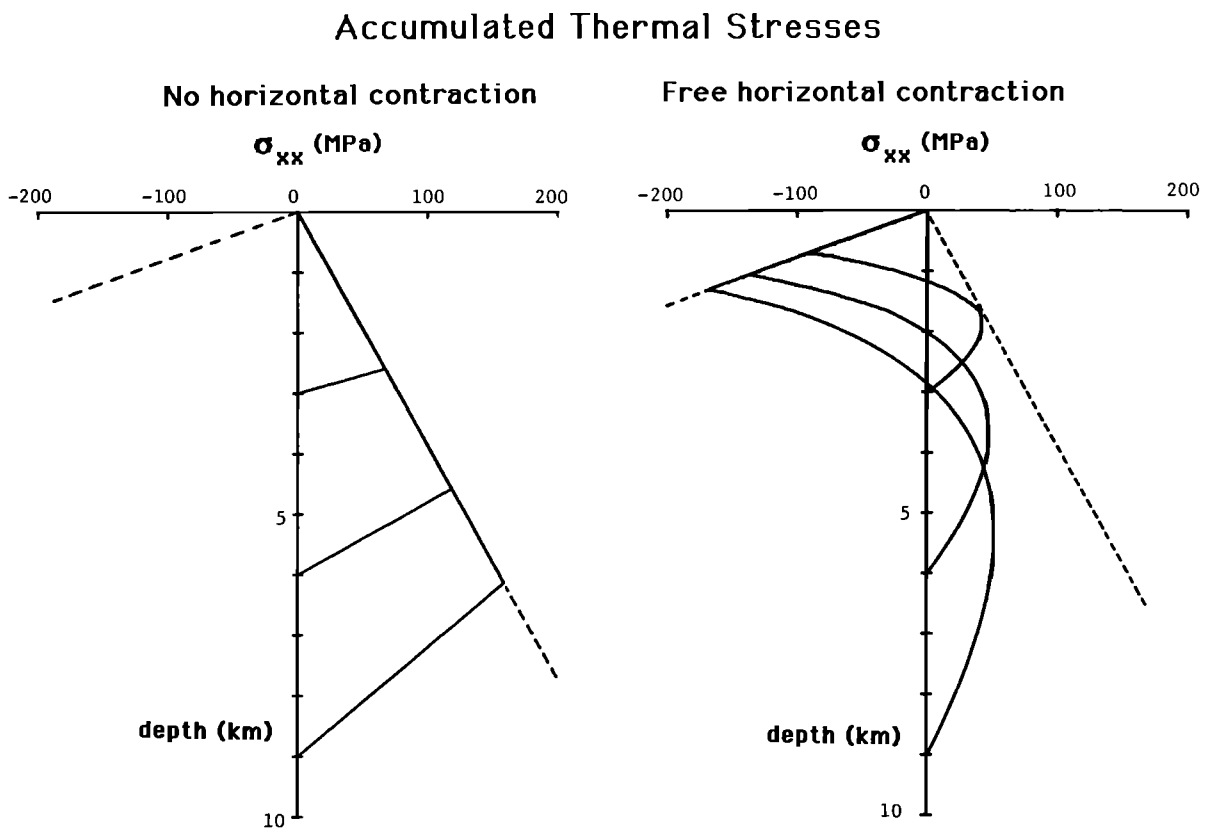

Fig. 2. Thermal stress distribution with depth in a brittle-elastic plate that progressively accumulate as the plate thickens [from *Parmentier and Haxby*, 1986]. The bottom of the brittle-elastic plate is defined by a prescribed temperature at which material begins to accumulate elastic stress on cooling. Brittle failure by faulting, shown by the dashed failure envelopes, limits the maximum stress that can accumulate. Stress distributions for three plate thickness are shown for the limiting cases of no horizontal contraction (left) and free horizontal contraction (right).

To simplify the calculation of thermal stresses, we consider a plate that is thin compared to its lateral dimensions and that thickens slowly with distance from the spreading center. In this case, approximately free contraction of the plate can occur in the vertical direction so that the vertical normal stress σ_{zz} as well as the shear stresses σ_{xz} and σ_{yz}, associated with x and y variations of the vertical normal stress, are small. The strains e_{xx} and e_{yy} are independent of z, which is equivalent to neglecting bending of the plate. Calculating the thermal contraction stresses thus reduces to the two-dimensional problem of solving for the variation of the vertically averaged stress components in the x and y directions.

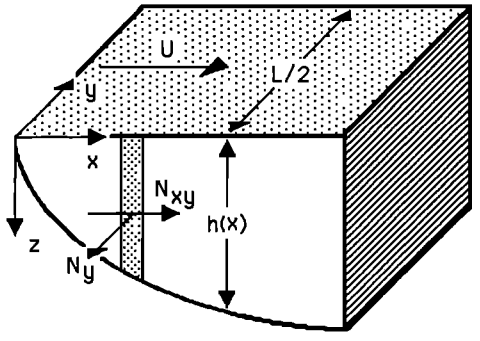

Fig. 3. Notation and coordinate system for the analysis of thermal contraction stresses in an elastic lithosphere that thickens with age.

As in our earlier treatment of thermal bending stresses, it is important to recognize that material added to the bottom of the elastic lithosphere in an increment of thickening is initially free of elastic stress and that elastic stress in material previously added to the thickening lithosphere accumulates progressively as the material cools. With the approximations described above, the incremental accumulation of stresses within a thickening, cooling plate can be calculated by considering the incremental stresses in a vertical slice of the plate parallel to the spreading center as it moves from a distance x to $x + \delta x$ from the spreading center. Using the constituitive equation for an elastic material with Young's modulus E, Poisson's ratio ν, and coefficient of linear expansion α [cf. *Timoshenko and Goodier*, 1970], the incremental strain is given by

$$\delta e_{xx} = (\delta N_{xx} - \nu \delta N_{yy} + \delta N_T)/Eh$$
$$\delta e_{yy} = (\delta N_{yy} - \nu \delta N_{xx} + \delta N_T)/Eh \quad (1)$$
$$\delta e_{xy} = (1 + \nu)\delta N_{xy}/Eh$$

where

$$\delta N_{ij} = n_{ij}\delta x = \int \delta \sigma_{ij}\, dz$$

$$\delta N_T = n_T \delta x = E\alpha \int \delta T\, dz$$

the integrations extending over the thickness of the plate from

$z = 0$ to h. The thickness integrated stresses N_{ij} represent forces per unit horizontal distance acting on vertical planes within the plate. To clearly distinguish them from stresses, we refer to these thickness integrated stresses as forces.

The incremental forces n_{ij} and the incremental strains δe_{ij} must satisfy the equilibrium equations and compatibility equation, respectively,

$$\partial n_{xx}/\partial x + \partial n_{xy}/\partial y = 0 \tag{2a}$$

$$\partial n_{xy}/\partial x + \partial n_{yy}/\partial y = 0 \tag{2b}$$

$$\partial^2(\delta e_{xx})/\partial y^2 + \partial^2(\delta e_{yy})/\partial x^2 - 2\partial^2(\delta e_{xy})/\partial x \partial y = 0 \tag{3}$$

Combining equations (1), (2), and (3) and introducing an Airy stress function gives a single differential equation for the incremental stress function f:

$$\nabla^2(\beta\nabla^2 f) - (1 + \nu)(\partial^2\beta/\partial x^2\ \partial^2 f/\partial y^2 + \partial^2\beta/\partial y^2\ \partial^2 f/\partial x^2 - 2\ \partial^2\beta/\partial x\partial y\ \partial^2 f/\partial x\partial y) = -\nabla^2(\beta n_T) \tag{4}$$

where $\beta = 1/h$ and

$$n_T = \alpha E \int \partial T/\partial x\, dz$$

the integral extending over the thickness of the plate. The incremental forces are obtained from derivatives of the stress function $n_{xx} = \partial^2 f/\partial y^2$, $n_{yy} = \partial^2 f/\partial x^2$, and $n_{xy} = -\partial^2 f/\partial x \partial y$. On boundaries where the normal and shear forces vanish, the corresponding stress increments must also vanish. These conditions are satisfied by making f and its normal derivative vanish along each edge of the plate. The stress within the plate is the accumulation of stress increments up to that age or distance from the ridge axis. Therefore, after solving for the incremental force field the stresses are obtained by integrating the incremental forces in the x direction and dividing the resulting thickness integrated stresses by the layer thickness

$$\sigma_{ij} = N_{ij}/h = \left[\int n_{ij}\, dx\right]\Big/ h \tag{5}$$

where the integration extends from $x = 0$ and the accumulated forces on this boundary vanish. *Sandwell* [1986] has also recently considered thermal contraction stresses in cooling oceanic lithosphere. Our treatment differs in that we explicitly treat stress accumulation and the effect of plate thickness variations.

The boundary value problem defined above is nondimensionalized by choosing a suitable characteristic length and stress. The plate width L, the only fixed length in the problem, is chosen as the characteristic length. Inserting the temperature and layer thickness distribution given above into equation (4) and nondimensionalizing the stress function by σL^2, where the characteristic stress $\sigma = \alpha E T_m[1 - \exp(-A^2)]/2A\pi^{1/2}$, gives

$$x^3\nabla^2(x^{-1/2}\nabla^2 f) - 3(1 + \nu)/4\ x^{1/2}\partial^2 f/\partial y^2 = 2 \tag{6}$$

Note that this equation, written in terms of nondimensional variables, contains no parameters that depend on σ, L, or U. The characteristic stress σ is simply the ridge parallel tensional stress that would occur throughout a plate in which the boundary conditions permit no contraction parallel to the ridge axis. For $\alpha = 10^{-5}$ °C^{-1}, $E = 100$ GPa, $T_l = 700$°C, and $T_m = 1200$°C, this stress will have a magnitude of about 300 MPa (3 kbar).

The solution to equation (6) may be evaluated analytically in two limiting cases. In the region near the ridge axis, $x \ll 1/2$, $|y| < 1/2$, where the nondimensional coordinate system is defined such that the transform boundaries are at $y = \pm 1/2$, the boundary conditions demand that the y derivatives of f vanish. In this region, equation (6) reduces to

$$x^3\partial^2[x^{-1/2}n_{yy}]/\partial x^2 = 2 \tag{7}$$

which is the differential equation that describes the state of stress in a cooling plate that is not allowed to contract horizontally in the ridge-parallel direction. As the ridge axis is approached along a flow line, the state of stress approaches uniaxial tension: for $y < 1/2$ and as x approaches zero, σ_{yy}, the ridge-parallel stress, asymptotically approaches the value σ above, and σ_{xx} vanishes. At large distances from the ridge axis, $x \gg 1/2$, the asymptotic solution to equation (6), obtained by expanding f in an even polynomial in y and retaining the lowest-order $1/x$ terms in each polynomial coefficient, is given by

$$f = x^{-5/2}\{y^4/12 - y^2/24 + 1/192 + O(1/x)\} \tag{8}$$

indicating that ridge-axis-parallel stresses decay much more rapidly with distance from the ridge than ridge-perpendicular stresses.

Equation (6) is solved using finite difference methods. Partial derivatives appearing in this equation are approximated by central finite difference derivatives leading to a system of algebraic equations consisting of one equation for each grid point. The solution of this system which satisfies the boundary conditions given above is obtained by a simple successive overrelaxation procedure. The accuracy of the finite difference solutions is determined by the spacing of grid points. We have employed uniformly spaced grid points with 89 grid points along the ridge axis between $y = 0$ and $1/2$ and 180 grid points in the spreading direction. At large values of x we used the analytic solution valid for $x \gg 1/2$, discussed above, as a boundary condition. Except for a small region near the corner of the plate representing the ridge-transform intersection, solutions for the stresses should be accurate to within a few percent. Near the corner the vanishing thickening of the plate near the ridge axis results in a discontinuity in the ridge-axis-parallel stresses that is smeared out over several grid points. The following results are calculated for $\nu = 0.25$.

RESULTS

The stress components σ_{ij} resulting from the finite difference solution of equation (6) are shown in Figure 4. The magnitude of the three tensor components referred to the x and y directions and normalized by the characteristic stress σ, given above, are shown in each figure. One important and immediate conclusion is that the magnitudes of the stress components shown in Figure 4 do not depend on the spreading rate or the ridge segment length. Furthermore, the variation of stresses with distance from the ridge scales directly with the ridge segment length but is independent of the spreading rate. This conclusion follows directly from the nondimensionalization described above. If the ridge-axis-parallel stress increased with the plate width, or the ridge segment length, it could be argued that a plate wider than some critical length would fail, forming a new fracture zone. However, since the stress is independent of the plate width, it is difficult to understand how the

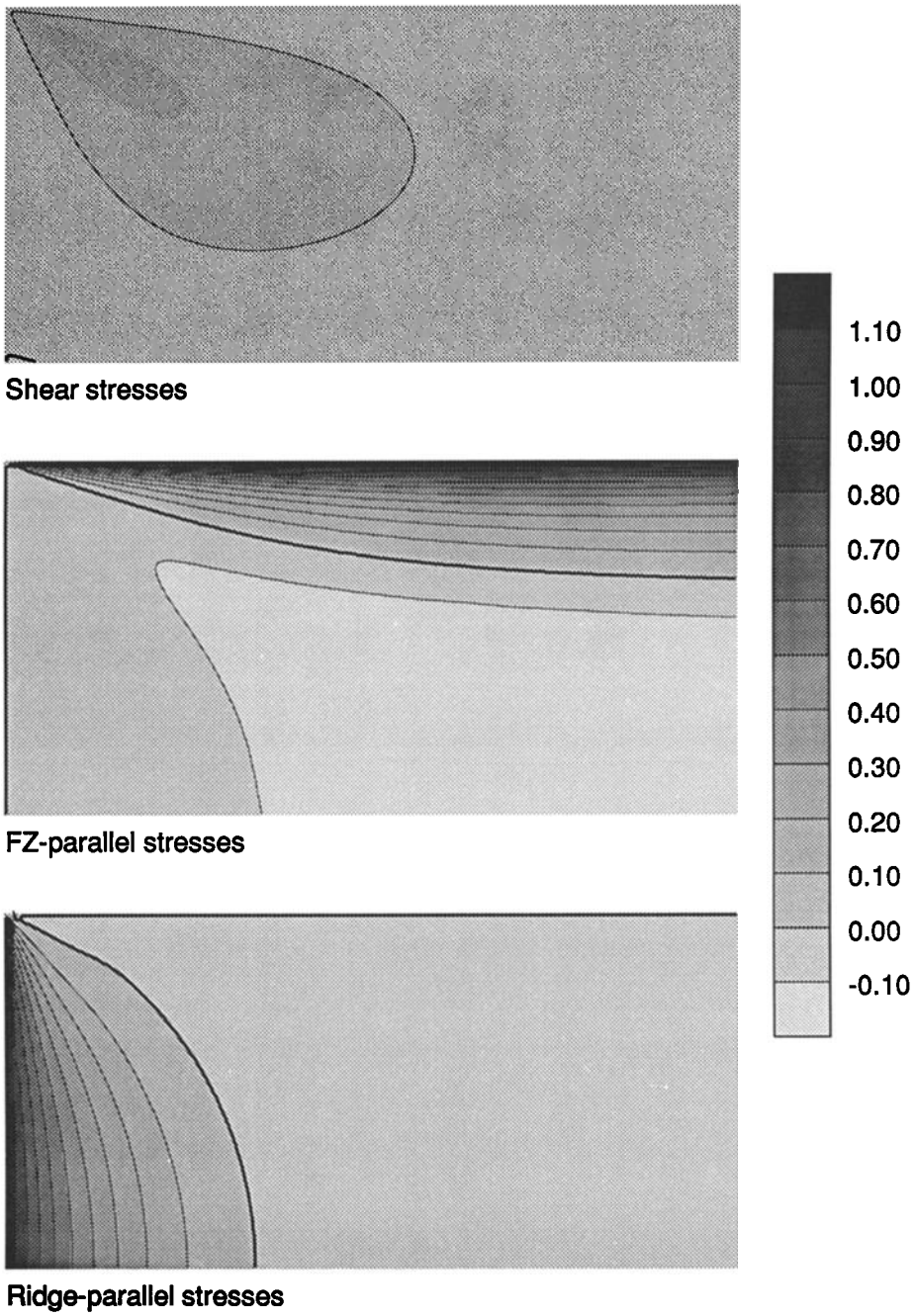

Fig. 4. Distribution of thermal contraction stresses in a plate that thickens away from a ridge axis. On each diagram, the ridge axis is on the left, and the bottom corresponds to the center of the plate about which the stress field is symmetric. The top of each diagram corresponds to the stress-free edge of the plate that we refer to as the FZ in this simple model. Stress magnitudes are represented as multiples of the chracteristic stress σ (discussed in text) which is expected to have magnitude of about 300 MPa (3 kbar).

ridge-parallel tensile stress alone can control the spacing of FZs.

The stress field, expressed as components parallel and perpendicular to the ridge axis, predicted by our model, is shown in Figure 4. The orientation and magnitude of the principal stresses and the maximum shear stress directions are shown in Figure 5. As shown in Figure 4, tensile, ridge-parallel thermal contraction stresses occur along the ridge axis, as would be expected. The largest value, which occurs near the center of the ridge segment at the ridge axis, is equal to the stress σ that would occur with no ridge axis-parallel contraction. Because the plate is very thin and cools very rapidly near the ridge axis, ridge axis-parallel horizontal contraction is prevented by its mechanical coupling to the thicker, more slowly cooling plate farther from the axis. Our numerical solutions attain this expected value within a few percent. However, large ridge-parallel tensile stresses occur only near the ridge axis. This stress component decreases to one tenth of its largest ridge axis value in a distance of only about $L/4$, and the plate interior is characterized by relatively small compressional

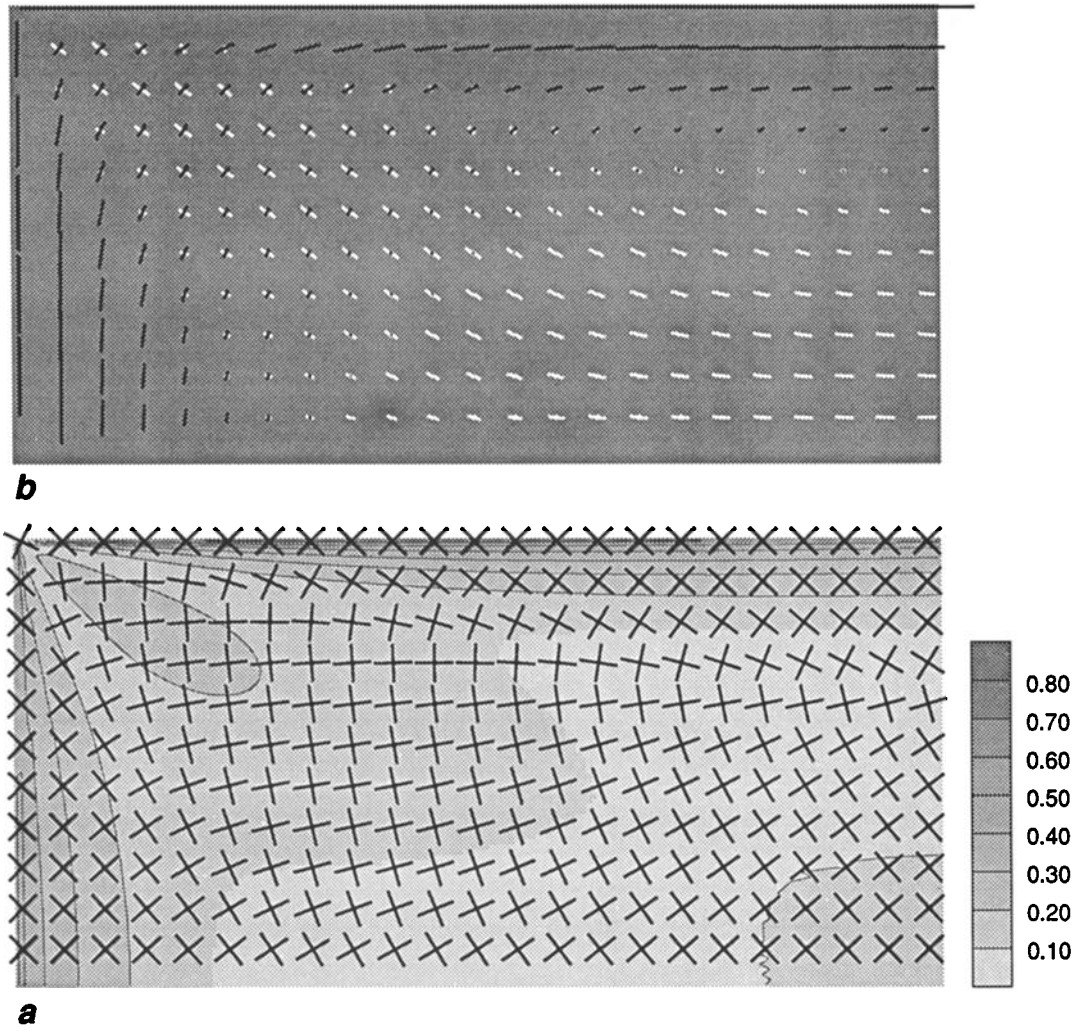

Fig. 5. Magnitudes and directions of the principal stresses and the maximum shear stress for the same arrangement of plate boundaries as in Figure 4. Stress magnitudes are again represented as multiples of the characteristic stress σ (discussed in the text).

stresses perpendicular to the ridge axis. Relatively large transform-parallel tensional stresses occur along the sides of the plate. The transform-parallel tensional stresses that our model predict attain a maximum value of about 1.25σ. This stress is greater than the ridge-axis-parallel stresses at the ridge axis and persists to a distance from the ridge of several ridge segment lengths. The maximum tensile stress occurs at a distance of about $L/2$ from the ridge. It is interesting to speculate that these stresses may help to control the length of transforms and that the high stress region may be a preferred site for ridge jumps or propagation.

Although the prediction of tensile ridge-axis-parallel stresses in our model is similar to that of *Sandwell* [1986], the results differ in several important respects. In our results, because the ridge-axis-parallel stress remains finite and the plate thickness vanishes, the ridge-axis-parallel force N_{yy} vanishes near the ridge axis. *Sandwell* [1986] imposed a vanishing ridge-axis-parallel force at the ridge axis, but his solution results in a finite shear force on the ridge axis contrary to the stated boundary condition of vanishing shear force there. His results also show transform-parallel compression along the transform edge of the plate in contrast to the tensional stresses in our model.

Thermal bending moments that develop in the presence of thermal contraction stresses are shown in Figure 6, and examples of the depth distribution of stresses that generate these moments are shown in Figure 7. As in our earlier study, these stress distributions result from the progressive accumulation of stress in a thickening plate that is not allowed to bend. The moments calculated from these stress distributions can then be viewed as loading which will bend the plate and accordingly modify the stress distributions. In the absence of bending, the maximum thermal stress exceeds the thermal contraction or vertically averaged stress. The maximum thermal bending stress is always comparable to or greater than the characteristic stress σ, even in regions of the plate where thermal contraction stresses are near zero. The moment of the ridge-parallel stresses will produce bending about an axis perpendicular to the ridge. Near the FZ and throughout the plate interior at distances greater $L/2$ from the ridge axis, the bending moment due to ridge-parallel stresses is essentially identical to the bending moment for free horizontal contraction. However, in the plate interior near the ridge axis the bending moment is less than the free contraction stresses would predict. This indicates that the results of our previous study, which assumed free contraction throughout the plate, would

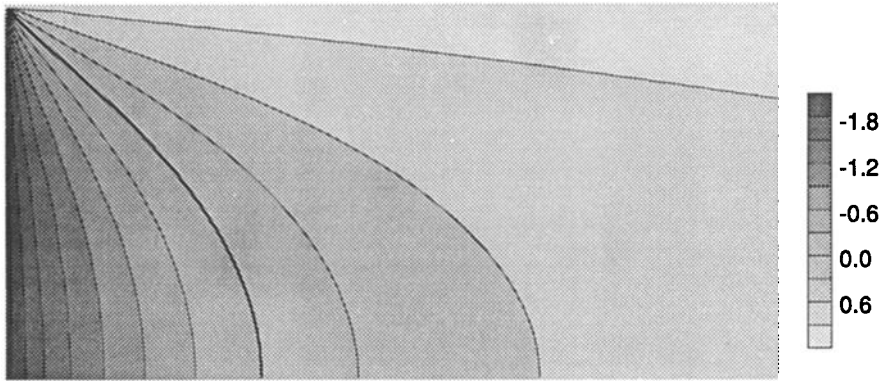

Fig. 6. Distribution of bending moments due to ridge-parallel stresses with depth distributions like those shown in Figure 7. Moments are represented as the indicated multiples of the moment $\alpha E T_1 h^2/24(1-\nu)$ for the free horizontal contraction stress distribution in a perfectly elastic plate [see *Parmentier and Haxby*, 1986]. Positive and negative moments cause concave downward and concave upward bending of the plate, respectively.

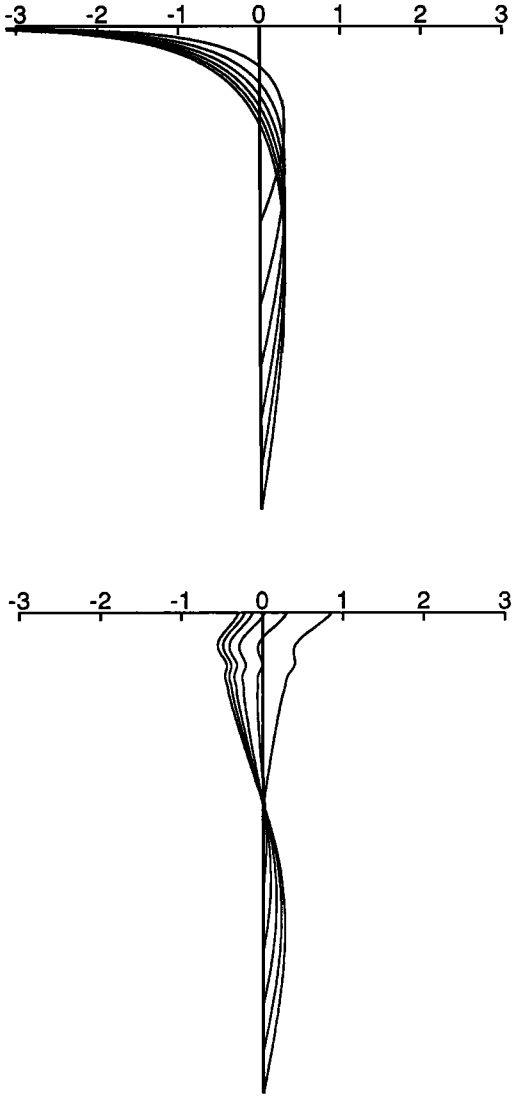

Fig. 7. Depth distributions of ridge-parallel normal stresses in a perfectly elastic plate along the FZ boundary, (top) $x = L/2$ and (bottom) along the center of the plate $x = 0$. In each diagram, distributions of stress are shown at six equally spaced distances from the ridge axis extending to a maximum distance of one ridge segment length $y = L$. In each case the stress vanishes at the bottom of elastic plate. Stress magnitudes are represented as multiples of the characteristic stress σ given in the text.

be affected only if the transform were much shorter than the ridge segment length and suggests a transform length dependence not included in our earlier thermal bending model. A two-dimensional formulation of the flexural model will be required to examine this effect. However, in the vicinity of a transform and throughout the plate interior at distance from the ridge axis greater than about one half of the ridge segment length, the thermal bending moments are well approximated by their free contraction values.

DISCUSSION

It is important to discuss several simplifications and assumptions in the model described above. First, in our calculation of thermal contraction stresses we have considered only a perfectly elastic plate. As illustrated by the simple limiting cases of free horizontal contraction and no horizontal contraction, shown in Figure 2, thermal stresses are expected to be large enough to cause brittle failure of the lithosphere, particularly at shallow depths beneath the seafloor. Failure therefore reduces the effective elastic lithosphere thickness. The general effect of failure will be to reduce the thermal contraction stresses, particularly the large ridge-axis-parallel tensile stress that occurs near the ridge axis. This has also been pointed out by *Sandwell* [1986]. Since the stresses within the plate away from the ridge axis reflect a combination of local cooling and stresses transmitted away from the region near the plate boundary, thermal contraction stresses will be reduced not only near the ridge axis but also throughout the plate. Thus the effect of thermal contraction stresses in reducing the thermal bending moment from its free contraction value will be less pronounced than indicated by the results in Figure 7.

Thermal stresses in the vicinity of the ridge axis will also depend on features of the thermal and mechanical structure of the ridge that we have not attempted to include in the present study. We have considered only the idealized thermal model in which the thermal boundary layer and plate thickness vanish at the ridge axis. However, several thermal models [*Sleep*, 1975; *Reid and Jackson*, 1981; *Morton and Sleep*, 1985; *Phipps Morgan et al.*, 1987] show that the thermal boundary layer and therefore a strong plate will have a finite thickness at the ridge axis. Observations of seismicity along ridge axes indicate that microearthquakes can occur at depths as great as

8–10 km on a slow spreading ridge like the mid-Atlantic Ridge [*Toomey et al.*, 1985].

If the plate were created with a finite thickness at the ridge axis, the ridge-axis-parallel stress would vanish since elastic stress could not accumulate instantaneously. In the present model, finite stress at the ridge axis is a consequence of the very rapid thickening of the plate. The plate at a ridge axis must form by the solidification and cooling of material magmatically emplaced on or very near the ridge axis. This cooling and solidification process will lead to the development of thermal stresses and perhaps bending of the plate. The along-axis deepening of ridges toward FZs and other ridge axis discontinuities has been attributed to the localization of magma emplacement near the center of a ridge segment [*Francheteau and Ballard*, 1983; *Whitehead et al.*, 1984; *Crane*, 1985] or by horizontal pressure gradients associated with viscous mantle flow at the ridge axis [*Parmentier and Forsyth*, 1985]. Thermal bending stresses at the ridge axis may also contribute to this along axis topography. While the nodal deep at ridge-transform intersections can be attributed in part to thinner crust, along the slow spreading Mid-Atlantic Ridge, deepening extends over the whole length of a ridge segment. There is no evidence that crustal thickness variations are responsible for this long 50- to 100-km wavelength deepening. The seismic data which do exist suggest that pronounced crustal thickness variations occur primarily within about 10 km of a FZ. Gravity and topography profiles across the Rio Grande FZ complex [*Gamboa and Rabinowitz*, 1981, Figure 2], for example, show that the observed topography cannot be isostatically compensated at depths of 6–8 km. Bending of the plate by thermal bending stresses may contribute to the ridge-transform intersection deep and associated topographic high that occurs in the ridge-transform corner [*Fox and Gallo*, 1984; *Kuo et al.*, 1984].

The present model as well as our earlier plate bending model assumes that a transform can be treated as a boundary across which there is no vertical or horizontal mechanical coupling of plates. The degree to which fault distributions and orientations are influenced by thermal stresses can provide a possible constraint on the mechanical coupling of plates across a transform. Fault scarps observed on the seafloor are generally oriented along the axis of the mid-ocean ridge reflecting plate extension associated with the spreading process [cf. *Macdonald*, 1982]. However, oblique or curving faults are observed near ridge-transform intersections [*Fox and Gallo*, 1984; *Macdonald et al.*, 1986] where normal faults on the transform side of the ridge axis curve away from the axis. These fault orientations near ridge-transform intersections may be explained by shear stresses on the transform [*Lonsdale*, 1977; *Fujita and Sleep*, 1978; *Fox and Gallo*, 1984; *Castillo and Macdonald*, 1984; *Phipps Morgan and Parmentier*, 1984; K. Crane and K. Fujita, unpublished manuscript, 1987]. The thermal contraction stresses shown in Figure 5 do not explain the observed fault patterns. As shown in Figure 5, the least compressive stresses near the corner representing the ridge-transform intersection are oblique to the ridge axis, but the calculated orientation would predict normal faults that extend radially from the ridge-transform corner, in contrast to the observed distribution. The normal stresses in the corner region are also relatively small, decreasing rapidly with distance from both the ridge axis and transform boundaries of the plate. If, alternatively, the plate were not free to contract at the transform boundary, the large ridge-axis-parallel tensional stress would extend off the axis into the corner region. These ridge-parallel stresses would surely be large enough to cause faulting in the plate but would not explain the observed change in fault orientation approaching a ridge-transform intersection. The observed pattern of faulting is thus consistent with the assumption that free horizontal contraction of the plates can occur across the transform. Both *Collette* [1974] and *Sandwell* [1986] have suggested that separation of plates along the transform may explain the presence of a FZ valley.

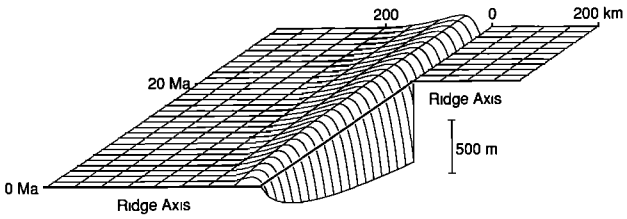

Fig. 8. General form of the seafloor topography predicted by thermal bending stresses. Bending of the plate by thermal stresses accumulates as the plate ages and thickens. The transform is assumed to be a free edge across which the plates are mechanically decoupled.

Assuming that adjacent plates are mechanically decoupled across a transform, thermal bending moments will cause flexure of the plate adjacent to this free edge. The general form of the thermal bending stress supported topography predicted previously [*Parmentier and Haxby*, 1986] is shown in Figure 8. Flexure accumulates as the plate cools and thickens with age along the transform. Assuming that plates are welded together along the inactive part of the FZ and that the plates thicken as the squareroot of age, no additional flexure of the plates occur along this part of the FZ. The topography that has accumulated along the transform remains frozen-in along the inactive part of the FZ. The resulting topography has the form of a topographic low immediately adjacent to the FZ and a broader topographic high on the old side. Seafloor topography of this form is, in fact, observed adjacent to FZs. A topography profile across the Udintsev FZ in the Antarctic plate and a nearby Seasat geoid profile are shown in Figure 9. There is a clearly defined asymmetric topographic low and a broader topographic swell on the old side of the FZ. The general form of the geoid anomaly corresponds well to this topography. Geoid and topography profiles across the Mendocino FZ, shown in Figure 10, also show a positive geoid anomaly as well as a topographic high on the old side of the FZ. Preliminary analysis of the geoid and topography indicates that this seafloor topography cannot be isostatically compensated at crustal thickness depths. Topography isostatically compensated by crustal thickness variations at a depth of 6 km would produce a geoid anomaly of about 35 cm per kilometer of seafloor topography [*Haxby and Turcotte*, 1978]. An approximately 500-m-high swell would produce a geoid high of only 17 cm, in contrast to the 50-cm or more high that is observed. Our previous study [*Parmentier and Haxby*, 1986] has shown that the observed geoid anomaly is well explained by uncompensated topography due to flexure by thermal bending moments.

An important objective of our studies of thermal stress is to understand mechanisms leading to the formation of FZs. Several studies cited earlier have hypothesized that FZs form in response to thermal contraction stresses. However, we have

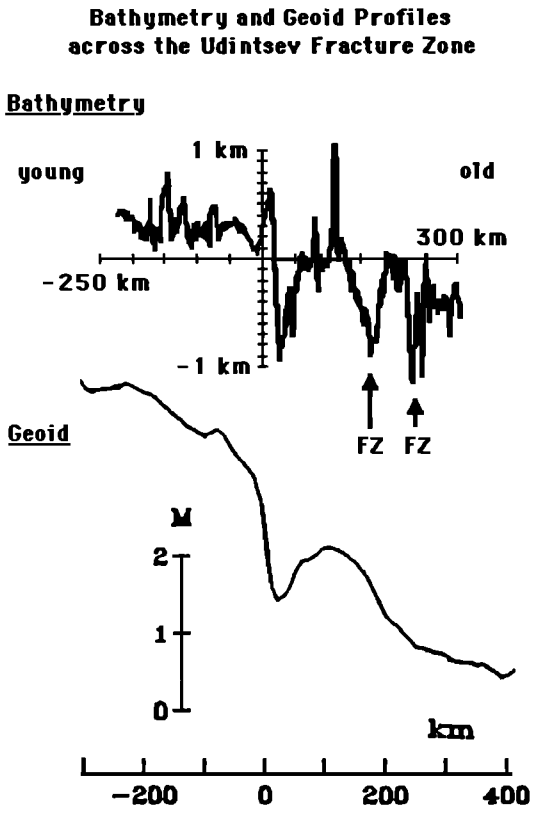

Fig. 9. Topography along a shiptrack crossing the Udintsev FZ at 135°W along with a nearby Seasat profile [*Parmentier and Haxby*, 1986, Figure 12*a*]. The shiptrack is projected normal to the FZ. The young side is on the left, and the prominent trough in the center of the profile is the FZ. Note the good correspondence between the topography and the Seasat geoid profile.

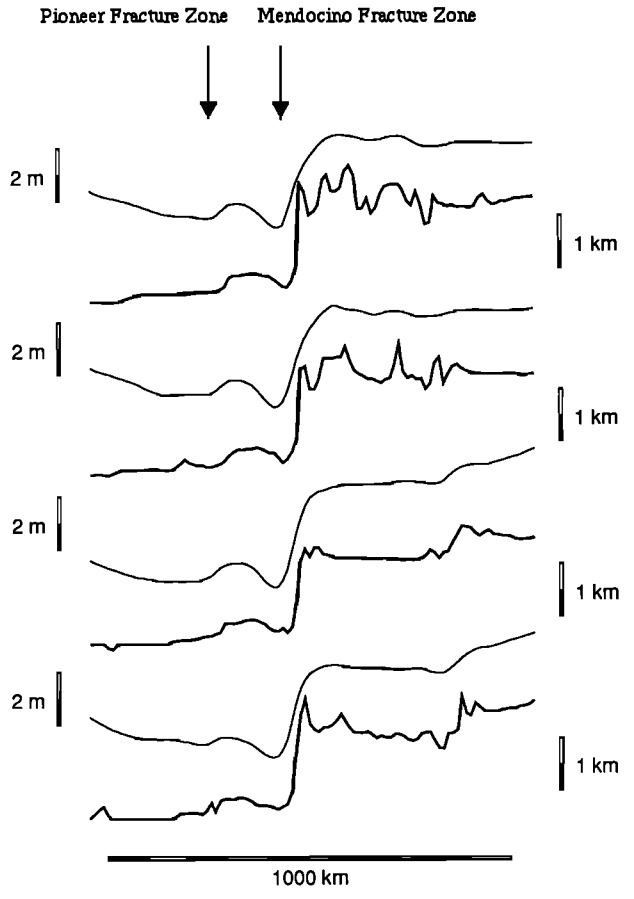

Fig. 10. Seafloor topography and geoid profiles across the Mendocino FZ at a number of locations along the FZ. The profiles were plotted from bathymetry and geoid data gridded at 10 arc min intervals. The amplitude of a narrow feature such as the FZ trough may be reduced by the gridding procedure, but the broader flanking high should be less affected. Plate flexure that we attribute to thermal bending stresses can be seen as the swell along the old (deep) side of the FZ trough. Note that this corresponds well with the geoid high also observed at the Clarion and Udintsev FZs [*Parmentier and Haxby*, 1986]. The Pioneer FZ occurs at the outer periphery of the thermal stress flexure. A possible explanation for the formation of a FZ in this location is shown in Figure 11.

recognized several examples of FZs which may be related to thermal bending stresses. One example is shown in Figure 9, where a small offset FZ occurs on the outer edge of the swell that we attribute to thermal bending. An even clearer example, shown in Figure 10, is the relationship between the Pioneer and Mendocino FZs: the Pioneer FZ again occurs on the outer edge of a swell on the old side of the larger offset Mendocino FZ. A possible explanation for this relationship is shown in Figure 11. Adjacent to a FZ where the plate is flexed concave downward, thermal bending stresses are relieved by the flexure. However, in the adjacent concave upward region, which must be present if the plate remains continuous, thermal bending stresses are enhanced by flexure. While thermal bending does not explain the development of shear offset on a growing FZ, it is not unreasonable to expect a new FZ to form in this highly stressed region of the plate.

CONCLUSIONS

Thermal contraction stresses, due to changes in the vertically averaged temperature and thickness of the oceanic lithosphere, accumulate as the lithosphere thickens with distance from a ridge axis. We have examined thermal contraction stresses in a simple semi-infinite rectangular plate which thickens as the square root of age and with free edges representing the transform faults. At the ridge axis, where the plate is very thin but thickening rapidly, no contraction of the plate parallel to the ridge axis can occur. This leads to large ridge-axis-

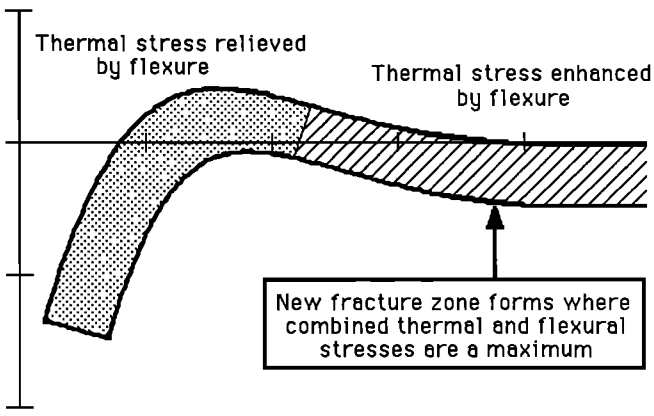

Fig. 11. Schematic diagram showing the region of highly stressed lithosphere at the outer edge of the peripheral swell adjacent to the old side of a FZ (see Figure 8). In this region, thermal bending stresses are not relieved by plate flexure. Based on examples discussed in the text, we postulate that this region is a likely site for the formation of a new fracture zone.

parallel thermal contraction stresses that decrease rapidly with distance from the ridge axis. Thermal contraction stresses decrease to one tenth of their ridge axis values in a distance from the ridge axis of only about one fourth of the ridge segment length, corresponding to the plate width in our simple model. Thus our results show that large ridge-axis-parallel thermal contraction stresses are confined to the vicinity of the ridge axis. Thermal contraction parallel to the ridge axis also induces large transform-parallel tensile stresses along the free edges of the plate representing the transform fault. These stresses achieve a maximum value at a distance from the ridge axis of about one half of the plate width and persist to great distances from the ridge axis. We suggest that these transform-parallel stresses may have important implications for ridge jumps or propagation and may control the length of transform faults.

Thermal contraction stresses influence the magnitude of the bending moment due to thermal bending stresses that accumulate in response to changes in the vertical temperature distribution in the thickening plate. Thermal bending moments in a plate that undergoes free horizontal contraction are large compared to those in a plate that does not contract horizontally. Where thermal contraction stresses are small, thermal bending moments achieve values corresponding to a plate that undergoes free horizontal contraction. Strong reductions of the thermal bending moment from its free contraction value will thus occur only in the immediate vicinity of the ridge axis. Thermal bending moments with free horizontal contraction are large enough to bend the oceanic lithosphere and explain important, previously unrecognized features of the geoid anomaly observed along fracture zones. In a recent study of geoid anomalies along the Udintsev and Clarion fracture zones we have shown that this geoid anomaly consists of a geoid high on the old side of a fracture zone and a geoid low approximately centered on the fracture zone [*Parmentier and Haxby*, 1986]. These features can be clearly identified in the geoid anomaly across many other Pacific fracture zones and provide important information on the state of thermal stress in the oceanic lithosphere. Bathymetric profiles across the Udintsev and Mendocino fracture zones show seafloor topography that corresponds well to the predicted geoid anomaly due to thermal bending. The relative amplitudes of the topography and geoid anomaly show that this anomaly cannot be explained by crustal thickness variations or other mechanisms of isostatic compensation at shallow depths beneath the seafloor. The geoid anomaly and bathymetry are consistent with the uncompensated seafloor topography predicted by thermal bending.

Thermal contraction stresses have been suggested as a mechanism for the formation of fracture zones [*Collette*, 1974; *Turcotte*, 1974; *Sandwell*, 1986]. If the ridge-axis-parallel tensile thermal stresses increased with the ridge segment length, then one could argue that a ridge segment should not be longer than some critical length corresponding to the strength of the plate. However, in a simple rectangular plate, ridge-axis-parallel thermal contraction stresses at the ridge axis are independent of the width of the plate, corresponding to the ridge segment length in this simplified model. We suggest instead that fracture zones may form in response to thermal bending stresses. Examples of small offset fracture zones adjacent to larger offset fracture zones have been identified, the clearest example being the Pioneer and Mendocino fracture zones. The Pioneer fracture zone occurs on the old side of the Mendocino fracture zone in the region where thermal bending adjacent to the Mendocino cannot relieve the thermal bending stresses. A small offset, less well-mapped fracture zone may occur adjacent to the Udintsev fracture zone. While it is far from clear that all fracture zones form by this or any other single mechanism, the flexural length of the plate provides a natural length scale that may govern the spacing of transforms created by thermal stresses.

Acknowledgment. This research was supported by the National Science Foundation under grant OCE 87-00527.

REFERENCES

Bergman, E. A., and S. C. Solomon, Source mechanisms of earthquakes near mid-ocean ridges from body waveform inversion: Implications for the early evolution of oceanic lithosphere, *J. Geophys. Res.*, *89*, 11,415–11,441, 1984.

Bratt, S. R., E. A. Bergman, and S. C. Solomon, Thermoelastic stress: How important as a cause of earthquakes in young oceanic lithosphere?, *J. Geophys. Res.*, *90*, 10,249–10,260, 1985.

Castillo, D. A., and K. C. Macdonald, Tensile crack growth simulation of oblique trending structures associated with rift-transform intersections (abstract), *Eos Trans. AGU*, *65*, 1082, 1984.

Cazanave, A., B. Lago, and K. Dominh, Thermal parameters of the oceanic lithosphere estimated from geoid height data, *J. Geophys. Res.*, *88*, 1105–1118, 1983.

Collette, B. J., Thermal contraction joints in a spreading seafloor as origin of fracture zones, *Nature*, *251*, 299–300, 1974.

Crane, K., The spacing of rift axis highs: Dependence on diapiric processes in the underlying asthenosphere?, *Earth Planet. Sci. Lett.*, *72*, 405–414, 1985.

Crough, S. T., Geoid anomalies across fracture zones and the thickness of the lithosphere, *Earth Planet. Sci. Lett.*, *44*, 224–230, 1979.

Detrick, R. S., Jr., An analysis of geoid anomalies across the Mendocino fracture zone: Implications for thermal models of the lithosphere, *J. Geophys. Res.*, *86*, 11,751–11,762, 1981.

Fox, P. J., and D. G. Gallo, A tectonic model for ridge-transform-ridge plate boundaries: Implications for the structure of oceanic lithosphere, *Tectonophysics*, *104*, 205–242, 1984.

Francheteau, J., and R. D. Ballard, The East Pacific Rise near 21°N, 13°N, and 20°S: Inferences for along-strike variability of axial processes of the mid-ocean ridge, *Earth Planet. Sci. Lett.*, *64*, 93–116, 1983.

Fujita, K., and N. H. Sleep, Membrane stresses near mid-ocean ridge-transform intersections, *Tectonophysics*, *50*, 207–221, 1978.

Gamboa, L. A. P., and P. D. Rabinowitz, The Rio Grande fracture zone in the western South Atlantic and its tectonic implications, *Earth Planet. Sci. Lett.*, *52*, 410–418, 1981.

Haxby, W. F., and D. L. Turcotte, On isostatic geoid anomalies, *J. Geophys. Res.*, *83*, 5473–5478, 1978.

Haxby, W. F., S. C. Cande, J. L. LaBrecque, and J. K. Weissel, Applications of Seasat data to South Atlantic and Indo-Atlantic tectonics (abstract), *Eos Trans. AGU*, *66*, 360, 1985.

Kuo, B.-Y., J. Phipps Morgan, and D. W. Forsyth, Asymmetry in topography of the crestal mountains near a ridge-transform intersection (abstract), *Eos Trans. AGU*, *65*, 274, 1984.

Lister, C. R. B., Differential thermal stresses in the Earth, *Geophys. J. R. Astron. Soc.*, *86*, 319–330, 1986.

Lonsdale, P., Near-bottom reconnaissance of a fast-slipping transform fault zone at the Pacific-Nazca plate boundary, *J. Geol.*, *86*, 451–472, 1977.

Macdonald, K. C., Mid-ocean ridges: Fine scale tectonic, volcanic, and hydrothermal processes within the plate boundary zone, *Annu. Rev. Earth Planet. Sci.*, *10*, 155–190, 1982.

Macdonald, K. C., D. A. Castillo, S. P. Miller, P. J. Fox, K. A. Kastens, and E. Bonatti, Deep-Tow studies of the Vema fracture zone, 1, Tectonics of a major slow slipping transform fault and its intersection with the Mid-Atlantic Ridge, *J. Geophys. Res.*, *91*, 3334–3354, 1986.

Morton, J. L., and N. H. Sleep, A mid-ocean ridge thermal model: Constraints on the volume of axial hydrothermal heat flux, *J. Geophys. Res.*, *90*, 11,345–11,353, 1985.

Parmentier, E. M., and D. W. Forsyth, Three-dimensional flow beneath a slow spreading ridge axis: A dynamic contribution to the deepening of the median valley toward fracture zones, *J. Geophys. Res.*, *90*, 678–684, 1985.

Parmentier, E. M., and W. F. Haxby, Thermal stresses in the oceanic lithosphere: Evidence from geoid anomalies at fracture zones, *J. Geophys. Res.*, *91*, 7193–7204, 1986.

Phipps Morgan, J., and E. M. Parmentier, Lithospheric stress near a ridge-transform intersection, *Geophys. Res. Lett.*, *11*, 113–116, 1984.

Phipps Morgan, J., E. M. Parmentier, and J. Lin, Mechanisms for the origin of mid-ocean ridge axial topography: Implications for the thermal and mechanical structure accreting plate boundaries, *J. Geophys. Res.*, *92*, 12,823–12,836, 1987.

Reid, I., and H. R. Jackson, Oceanic spreading rate and crustal thickness, *Mar. Geophys. Res.*, *5*, 165–172, 1981.

Richardson, R. M., S. C. Solomon, and N. H. Sleep, Tectonic stress in the plates, *Rev. Geophys.*, *17*, 981–1019, 1979.

Sandwell, D., Thermal stress and the spacings of transform faults, *J. Geophys. Res.*, *91*, 6405–6417, 1986.

Sandwell, D., and G. Schubert, Geoid height-age relation from Seasat altimeter profiles across the Mendocino fracture zone, *J. Geophys. Res.*, *87*, 3949–3958, 1982.

Sleep, N. H., Formation of the oceanic crust: Some thermal constraints, *J. Geophys. Res.*, *80*, 4037–4042, 1975.

Sykes, L. R., and M. L. Sbar, Focal mechanism solutions of intraplate earthquakes and stresses in the lithosphere, in *Geodynamics of Iceland and the North Atlantic Area*, edited by L. Kristjansson, pp. 207–224, D. Reidel, Hingham, Mass., 1974.

Timoshenko, S. P., and J. N. Goodier, *Theory of Elasticity*, 3rd ed., 567 pp., McGraw-Hill, New York, 1970.

Toomey, D. R., S. C. Solomon, G. M. Purdy, and M. H. Murray, Microearthquakes beneath the median valley of the Mid-Atlantic Ridge near 23°N: Hypocenters and focal mechanisms, *J. Geophys. Res.*, *90*, 5443–5458, 1985.

Turcotte, D. L., Are transform faults thermal contraction cracks?, *J. Geophys. Res.*, *79*, 2573–2577, 1974.

Turcotte, D. L., and E. R. Oxburgh, Mid-plate tectonics, *Nature*, *244*, 337–339, 1973.

Whitehead, J. A., H. J. B. Dick, and H. Schouten, A mechanism for magmatic accretion under spreading centers, *Nature*, *312*, 146–148, 1984.

Wiens, D. A., and S. Stein, Age dependence of oceanic intraplate seismicity and implications for lithospheric evolution, *J. Geophys. Res.*, *88*, 6455–6468, 1983.

Wiens, D. A., and S. Stein, Intraplate seismicity and stresses in young oceanic lithosphere, *J. Geophys. Res.*, *89*, 11,442–11,464, 1984.

W. F. Haxby, Lamont-Doherty Geological Observatory, Palisades, NY 10964.

E. M. Parmentier, Department of Geological Sciences, Brown University, Providence, RI 02912.

(Received May 21, 1987;
revised September 10, 1987;
accepted November 19, 1987.)